Thermal Metallization of Silver Stearate-Coated Nanoparticles Owing to the Destruction of the Shell Structure

Nianjun Yang, Koichi Aoki,* and Hiroshi Nagasawa[†]

Department of Fiber Amenity Engineering, University of Fukui, 3-9-1 Bunkyo, Fukui-shi, 910-8507 Japan

Received: May 12, 2004; In Final Form: July 19, 2004

Nanoparticles composed of a silver stearate shell and a silver core became metallic bulk silver by heating at a temperature (340 °C) lower than the melting point of silver metal (960 °C). The metallization was investigated by thermogravimetric analysis, difference thermogravimetric analysis, FT-IR and UV−vis spectroscopy, electrochemical techniques, scanning electron microscopy, and measurements of the density of the nanoparticles. The nanoparticles decreased in mass by 20%, which was equivalent to the amount of the stearate shell. The low-temperature metallization resulted from the thermal decomposition of the shell of silver stearate into silver species. It involved two steps. The first, occurring at 250 °C, was the decomposition to porous silver particles through the first-order reaction with an activation energy of 111 kJ mol^{-1}. The second, occurring at 340 °C, was a structure change from porous particles to silver bulk crystals.

Introduction

Heating processes of mono-[1] and bimetallic[2] nanoparticles have recently been of great interest because they have the potential to exhibit fascinating properties different from those of bulk metals.[3] The well-known observation of thermal properties of metal nanoparticles is a decrease in the melting point with a decrease in size.[1] For example, Takagi[4] found as early as 1954 by the use of transmission electron microscopy that the melting point of gold nanoparticles decreased by 300 °C from the bulk melting point. Buffat and Borel[5] observed the dependence of the melting point of gold nanoclusters in a holey carbon grid on particle size by means of selected-area diffraction. Andres et al.[6] found a decrease in the melting point of gold nanoparticles by as much as 40% of that of the bulk. Schmidt et al.[7] reported that the melting point of Na_{139} nanoclusters 2.2 nm in diameter was 28% lower than that of bulk sodium. A melting-point depression of 31% was found by Allen et al.[8] for islands of Sn nanoparticles 10 nm in diameter using scanning nanocalorimetric analysis. However, an inverse phenomenon was reported for tin clusters[9] because their structure was different from that of the bulk. Gold nanoparticles smaller than 2.0 nm were reported not to vary their melting points.[6]

Thermodynamic models[10−15] have been proposed to account for the dependence of the melting point on the size of the nanoparticles. It has been commonly recognized that the surface atoms have quite different properties from the inside atoms. The decrease in the melting point is due to the large surface energy coming from the large specific surface area. In 1909, Pawlow[10] was the first to derive the quantitative relationship between the melting point and the particle size on the basis of the classical Kelvin equation. Pawlow predicted that the melting point had a linear relation with respect to the inverse of the diameter of the particle. Buffat and Borel[4] modified Pawlow's equation to predict the nonlinear decrease in the melting point with the inverse of the diameter. Theory has been gradually improved[11] with the aim of agreement with the experimental results. Kofaman et al.[12] and Sakai[13] presented surface premelting models in which the particle began to melt from the surface atoms and then abruptly fused over the inside. On the basis of the Landau theory, they explained the nonlinear relationship between the melting point and the inverse of the radius of particles as a surface curvature effect. Beck et al.[14] and Honeycutt et al.[15] pointed out that an assembly of small particles in the melting region is a mixture of solidlike and liquidlike forms. A predominant cause of the low melting points is reportedly due to not only the thermodynamic change in the melting temperature but also the enhancement of the latent heat of fusion.[16]

Most theories on the lower shift of melting points have been based on the surface energy of nanoparticles caused by curvature effects combined with interfacial phase effects. Because nanoparticles are dispersed against aggregation with the help of surfactants, it is important to take into account chemical effects of surfactants (e.g., desorption of surfactants from the surface of nanoparticles or decomposition of surfactants). We have observed[17] the significance of surfactants in silver nanoparticles dispersed in organic solvent through electrochemical measurements. The silver stearate-coated nanoparticle[17] is composed of a core of silver atoms and a shell of silver stearate. The shell was reduced to silver metal at −0.6 V, a more positive potential than that used for the silver stearate molecule (at −1.5 V). The positive potential shift indicated that the silver stearate of the nanoparticle has higher energy than the silver stearate molecule. Consequently, the nanoparticle is expected to fuse at a temperature lower than the melting point of bulk silver. This expectation stimulates us to heat the silver nanoparticle to find the role of the shell of silver stearate. In this paper, we report heated states of silver nanoparticles by means of UV−vis and FT-IR spectroscopy, scanning electron microscopy, thermogravimetric analysis, difference thermogravimetric analysis, and electrochemical techniques.

Experimental Section

All of the chemicals were of analytical grade. The silver stearate nanoparticles were synthesized with the method reported

* Corresponding author. E-mail: d930099@icpc00.icpc.fukui-u.ac.jp. Tel: +81-776-278665. Fax: +81-776-278494.
† Current address: Development Department 2, Development Center 2, Ebara Corp.
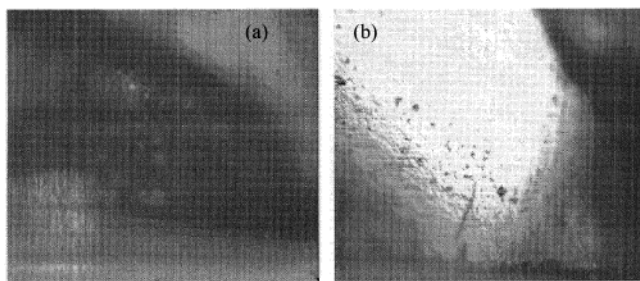
Figure 1. Photographs of (a) the unheated nanoparticle and (b) the nanoparticle heated to 340 °C for 5 min in the air. They were obtained by an optical microscope.

Figure 2. FT-IR spectra of (a) stearate acid, (b) silver stearate, (c) the nanoparticle, and (d) the nanoparticle heated to 340 °C for 5 min in the air. These samples were mounted in KBr pellets.

elsewhere.[18] Their average diameter (5 nm) and the size distribution (from 1 to 9 nm) were the same as those reported previously.[17,18] The crystal-like nanoparticles were dissolved in cyclohexane. The solution was dispersed on a glass plate or an indium−tin oxide (ITO)-coated glass plate and dried to form films.

UV−vis spectroscopy of the nanoparticle film was carried out at room temperature on a UV-570 spectrometer (JASCO, Tokyo). FT-IR spectra were recorded with 2-cm^{-1} resolution on a Protege 460 FT-IR instrument (Nicolet, Japan) at room temperature. A specimen for the analysis was prepared as a KBr pellet of dry samples.

Scanning electron microscopy (SEM) was performed with an SEM&EDX integration system (Hitachi). The samples were prepared directly on a copper substrate coated with carbon film.

Electrochemical experiments were made with a model 1112 potentio/galvanostat (Huso, Kawasaki) controlled by a computer. The reference and the counter electrodes were Ag|Ag$_x$O and platinum wire, respectively. The potential difference between Ag|Ag$_x$O and Ag|AgCl in 3 M NaCl was −0.055 V. The working electrode was a platinum disk electrode or an ITO plate.

Thermogravimetric analysis (TGA) and difference thermogravimetric analysis (DTA) were simultaneously applied to the dried powder of the nanoparticle (8−12 mg) with a computer-controlled DTG-60 apparatus (Shimazu, Kyoto). Temperature was scanned from room temperature to 500 °C at some heating rates (2, 5, 10, 20, 50 °C min^{-1}). Temperature was monitored with a thermocouple located near the chamber under a nitrogen atmosphere.

The density of aggregation of heated nanoparticles was evaluated from the mass and the excluded volume in a 10-cm^3 water vessel. The weighed aliquot (ca. 10 mg) of the nanoparticle was sunk in water, and the increment of the meniscus was read.

Results and Discussion

Decomposition of the Nanoparticles. The crystal-like nanoparticles heated to 340 °C for 10 minutes were aggregated into a lump. When the nanoparticle powder was dispersed on the ITO electrode by dropping nanoparticle-included cyclohexane solution and was heated to 340 °C, it became a thin film on the ITO. Figure 1 shows photographs of nanoparticles (a) before and (b) after heating, obtained by an optical microscope. The film before heating showed a rough, black surface. The film after heating to 340 °C for several minutes in air showed a smooth and brilliant surface (Figure 1b), as if it were a flattened droplet like fused solder. The film cooled to room temperature exhibited a white surface. An increase in the heating temperature reduced the time of the color change from black to brilliant. Because the nanoparticle involves silver stearate as a
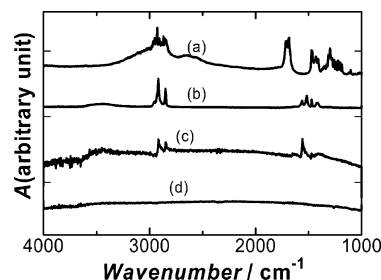
shell, the color change may be due to not only metallization but also the thermal decomposition of silver stearate.

To find participation in the thermal decomposition of silver stearate in the nanoparticle, FT-IR spectra of stearic acid, the silver stearate molecule, the nanoparticle, and the heated nanoparticle were obtained and are shown as curves (a)−(d) in Figure 2, respectively. The band at 1750 cm^{-1} that is attributed to the functional group of −COOH was observed only in curve (a). A series of bands in curves (a) and (c) in the domain of 2850−2970 cm^{-1}, which are attributable to the stretching of the CH$_2$ groups and the terminal CH$_3$ group, were not observed in curve (d) for the heated nanoparticle. The bands in the region of 1550−1620 cm^{-1} for COO$^-$ in curves (a)−(c) were not found in curve (d) either. Therefore, the increase in temperature up to 340 °C removes the stearate moiety from the nanoparticle. A plausible reaction mechanism is the thermal decomposition of silver stearate to silver metal and gases in the shell:

$$AgOOC(CH_2)_{16}CH_3 \rightarrow Ag + gas \qquad (1)$$
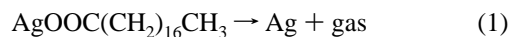
The final products of the gas should be CO$_2$ and H$_2$O because heating was done in air. Because the formation free energy of silver oxide is positive at temperatures greater than 200 °C,[19] silver metal is more stable than its oxide.

Reaction 1 suggests either the case in which all of the shell disappears in the gas or the shell is left as Ag metal. To obtain a reasonable reaction mechanism, we weighed the nanoparticles before and after heating. The nanoparticle decreased in mass by 20%, for example, from 15.6 to 12.5 mg, when it was heated to 340 °C and cooled to room temperature. We assume that the loss of mass is ascribed only to the gasification (the second case). Letting the number of silver stearate molecules in the shell be n_{Ag18}, that of the silver atoms in the core be n_{Ag}, the molar mass of silver stearate be M_{Ag18} (= 391 g mol^{-1}), and that of silver be M_{Ag} (= 108 g mol^{-1}), we can express the mass of the nanoparticle before and after heating as ($n_{Ag18} M_{Ag18}$ + $n_{Ag} M_{Ag}$) and ($n_{Ag18} + n_{Ag}$) M_{Ag}, respectively. These expressions correspond to 15.6 and 12.5 mg. Taking the ratio, we obtain the molar fraction of silver stearate, $n_{Ag18}/(n_{Ag18}+ n_{Ag})$, to be 0.095. The resulting ratio, n_{Ag}/n_{Ag18} (= 9.5), is close to the previously reported results (9.6).[17] Consequently, we can demonstrate quantitatively that the shell is decomposed into silver metal that is left on the silver core when the nanoparticles are heated to temperatures greater than 340 °C.

Figure 3 shows the cyclic voltammogram for the heated film in aqueous solutions (curve (a)). A clear anodic peak at 0.15 V appeared only in the first scan when the scan started at a potential less than 0.0 V. Thus, the anodic reaction is irreversible. The peak current increased with an increase in the number of dispersed nanoparticles on the ITO. As a control experiment, voltammetry of an aqueous AgNO$_3$ solution was carried out at a platinum electrode, and its wave is shown as curve (c). Ag$^+$

Thermal Metallization of Coated Nanoparticles

*J. Phys. Chem. B, Vol. 108, No. 39, 2004* **15029**
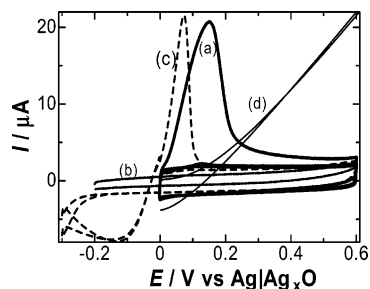
Figure 3. Cyclic voltammograms of (a) the nanoparticle film heated to 340 °C on the ITO electrode, (b) the unheated nanoparticle film, (c) 0.01 M silver nitrate at the Pt electrode, and (d) the silver wire electrode in a 0.1 M KNO$_3$ solution. They were obtained at the scan rate of 0.1 V s^{-1}. The current scales in curves (c) and (d) are $^1/_8$ and $^1/_{100}$ of the original scales, respectively.
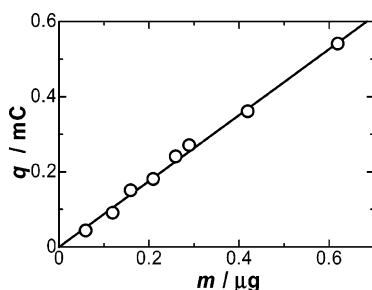
Figure 4. Dependence of the charge for the nanoparticle film heated to over 340 °C obtained from the anodic wave at 0.15 V on the mass of the nanoparticle film.

begins to be deposited for $E < -0.2$ V at the negative scan and continues to be deposited for $E < -0.03$ V at the positive scan. The deposited silver is dissolved at 0.1 V. This dissolution wave is similar to the anodic wave in curve (a). Consequently, the heated products should be mainly silver metal, as predicted. We found that the shape and the potential of the anodic wave were independent of the heating rate (2−50 °C min^{-1}) and the heating time (30−1800 s). The anodic wave of the heated nanoparticle was broadened and more shifted by 80 mV than the peak of curve (a). The broadness and the shift suggest the involvement of impure silver compounds owing to the decomposition of silver stearate or the difference in crystalline structure of silver metal. The FT-IR spectrum (curve (d) in Figure 2) shows no evidence of any organic impurity. A silver wire, whose crystalline structure may be different from that of the electrochemically deposited silver and the heated nanoparticle, showed a broad anodic dissolution wave (curve (d) of Figure 3). Therefore, the broadness and the shift in curve (a) are ascribed to the difference in the crystalline structure. The unheated film exhibited no voltammetric wave (curve (b)). This is consistent with the voltammograms of the nanoparticle-dissolved solution.[17] The absence of any wave is due to the protection of the redox reaction by the silver stearate shell.[17]

To confirm the heat-generated species on the ITO surface, we obtained a relation between the electrochemical charge, q, of the heated nanoparticle and the dry mass, m, of the mounted nanoparticle before heating. The charge was evaluated from the area of the anodic wave at 0.15 V. Figure 4 shows the variation of q with m, indicating proportionality. If the nanoparticles were to be made of only silver metal, then the slope, $^q/_m$, should be equal to F/M_{Ag}, where F is the Faraday constant. Values of $^q/_m$ in Figure 4 and F/M_{Ag} (= 96 485/108 C g^{-1}) are 755 and 893 C g^{-1}, respectively. The difference may be due to the assumption of only silver as the composition. We consider now the
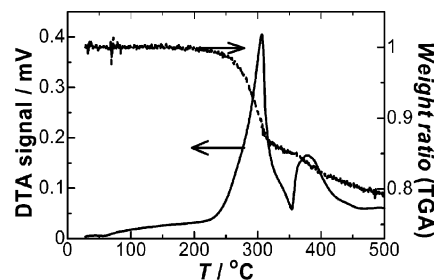
Figure 5. TGA and DAT curves for the nanoparticle from 25 to 500 °C at a heating rate of 10 °C min^{-1} under a nitrogen atmosphere.

participation in the shell of silver stearate more accurately for the previous observation[17] that the core and the shell are composed of silver and silver stearate, respectively. The charge and the mass of the nanoparticle are expressed by the participation in the core and the shell:

$$q = F(n_{Ag} + n_{Ag18}) \qquad (2)$$

$$m = n_{Ag}M_{Ag} + n_{Ag18}M_{Ag18} \qquad (3)$$

Then $^q/_m$ is given by

$$\frac{q}{m} = \frac{F(n_{Ag}/n_{Ag18} + 1)}{(n_{Ag}/n_{Ag18}) M_{Ag} + M_{Ag18}} \qquad (4)$$

By using $n_{Ag}/n_{Ag18} = 9.5$ obtained from the mass change by heating, the value on the right-hand side in eq 4 is 716 C g^{-1}. This value is smaller than the slope, q/m, by only 5%, as shown in Figure 4. This is because of the involvement of not only the capacitive component in q but also insufficiently positive potential to complete the dissolution of all of the silver metal, as was shown in difference curves (a) and (d) in Figure 3. All of these observations demonstrate that the shell of the nanoparticle is decomposed into pure silver when the heating temperature is greater than 340 °C.

Nonisothermal Kinetics of the Decomposition. To investigate the kinetics of the thermal decomposition of the shell, thermogravimetric analysis (TGA) and differential thermogravimetric analysis (DTA) were performed simultaneously, and their curves are shown in Figure 5. The TGA curve showed that the mass started to decrease at 230°C and reached the other state passing through a transition at 330 °C. The ratio of the mass decrease was 20% when the temperature increased to 500 °C. This ratio was consistent with the loss of mass by means of the long-time heating at 340 °C described in the previous section. The DTA curve showed two exothermic peaks at 306 and 380 °C. The former peak may be attributed to the decomposition of the shell, according to reaction 1. The latter peak may be caused by a phase transition of grain silver metal into silver bulk crystals, as will be mentioned from UV spectra and the SEM images in a later section.

Figure 6 shows the TGA curves at several heating rates. The transition temperature increased with an increase in the heating rate. The temperature at the peak of the DTA curves (not shown) also shifted toward higher temperature as the heating rate increased. The shift suggests a delay in the decomposition due to slow kinetics.

It is not easy to analyze a TGA curve accurately because of some instrumental limitations such as heat transport, location of the thermometer, uniformity of the temperature, and heat supplied by exothermic or endothermic reactions. However, kinetics can be roughly estimated from the TGA curves if the reaction order is known.[20] The decomposition of the shell is

15030 *J. Phys. Chem. B, Vol. 108, No. 39, 2004*

Yang et al.
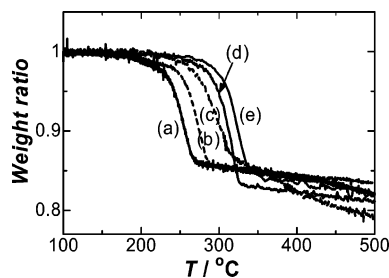
Figure 6. TGA curves at heating rates of (a) 2, (b) 5, (c) 10, (d) 20, and (e) 50 °C min^{-1}.
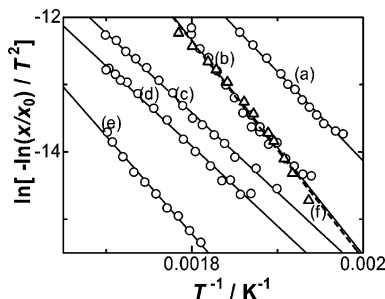
Figure 7. Plots of the left side of eq 8 against T^{-1} for curves (a)−(e) in Figure 6 and for the TGA curve of the monomer of silver stearate (f).

assumed to follow first-order kinetics, as in reaction 1. Letting x be the moles of silver stearate molecules in the shell, we can write the Arrhenius-type kinetic equation as

$$\frac{\mathrm{d}x}{\mathrm{d}t} = -A\mathrm{e}^{-(U/RT)}x \qquad (5)$$

where A is the frequency factor and U is the activation energy. Applying the linear heating scan condition, $T = T_0 + vt$, to eq 5 and integrating the resulting equation leads to

$$\ln\frac{x}{x_0} = \frac{AU}{Rv}\int_{U/RT_0}^{U/RT} \frac{\mathrm{e}^{-z}}{z^2}\,\mathrm{d}z \qquad (6)$$

where T_0 and x_0 are the initial temperature and the initial number of moles, respectively. If we assume that the variation of e^{-z} is much larger than that of z^{-2} and that $T_0 > T$ then eq 6 becomes

$$\frac{-\ln(x/x_0)}{T^2} = \left(\frac{AR}{vU}\right)\mathrm{e}^{-(U/RT)} \qquad (7)$$

or

$$\ln\left[\ln\left(\frac{x_0}{x}\right)\right] - 2\ln T = \ln\left(\frac{AR}{vT}\right) - \frac{U}{RT} \qquad (8)$$

Values of x/x_0 were obtained from TGA curves using

$$\frac{x}{x_0} = \frac{m_t - m_f}{m_0 - m_f} \qquad (9)$$

where m_0, m_t, and m_f are the initial mass, the mass at t, and the final mass of the samples, respectively. Plots of $\ln[(\ln(x_0/x))/T^2]$ versus T^{-1} are shown in Figure 7 at several values of the scan rate. They fall on a straight line over the domain for the conditions at each heating scan rate. The deviation from the line at high temperature may be ascribed to the instrumental limitations of TGA and the assumptions in the derivation. If we draw a straight line on the plot for each scan
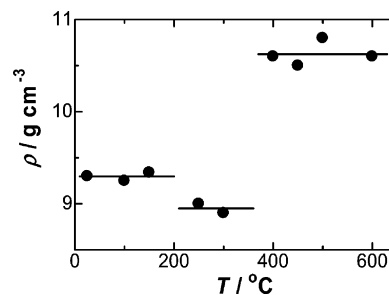
Figure 8. Temperature dependence of the densities of the nanoparticles, heated to several temperatures.

rate, then we obtained the activation energy $U = 111 \pm 20$ kJ mol^{-1}. The TGA measurement of molecular silver stearate was also made as a control experiment, and its logarithm plot is inserted into Figure 7. The activation energy $U = 108 \pm 14$ kJ mol^{-1} was close to the value for the nanoparticles. Consequently, the thermal variation of the nanoparticles at 340 °C is caused by the decomposition of silver stearate to silver in the shell.

Process of the Decomposition of the Nanoparticles. The density of the nanoparticles heated to several temperatures was evaluated by their weight and volume at room temperature. The volume was evaluated by the excluded volume of water when nanoparticles were sunk in water. Because a lump of nanoparticles has a hydrophobic surface, it floated on the water surface. It sank in water, however, after vigorous mixing for several minutes. Figure 8 shows the variation of the density with heating temperature. The density remains constant (9.3 g cm^{-3}) at temperatures lower than 200 °C. It decreased from 9.3 to 9.0 g cm^{-3} for $200 < T < 340$ °C and then increased to 10.5 g cm^{-3} for $T > 340$ °C. This increase was observed even at 250 °C when the heating time was longer than 20 min.
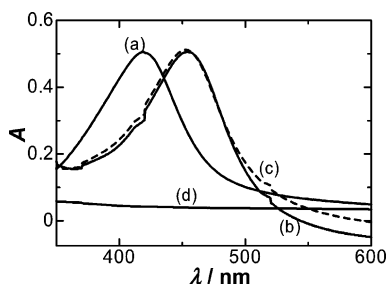
We shall explain the variation of the density from 9.5 to 9.2 g cm^{-3} quantitatively in terms of the decomposition of the shell. The density of a sphere with mass m and radius r is proportional to mr^{-3}. The diameters of the nanoparticle and its core are 5.3 and 5 nm, respectively, as estimated previously.[17] The density of the nanoparticle is proportional to $m(5.3)^{-3}$. The gas-removed nanoparticle may be close to the core in size. Therefore, the density is proportional to $0.8m(5)^{-3}$ when considering the 20% mass loss. Taking the ratio of the two densities yields 0.95, which is close to the value ($0.97 = 9.0/9.3$) obtained from the density in Figure 8. The product by the decomposition has a lower density (9.0 g cm^{-3}) than the silver crystals (10.5 g cm^{-3}), and hence it should have porous structure. Pores are necessarily produced because reaction 1 involves gas formation. The increase in the density from 9.0 to 10.5 g cm^{-3} over 340 °C may be due to the structural change from the porous structure to silver bulk crystals (10.5 g cm^{-3}) associated with an exothermic reaction, as shown in the DTA curve (Figure 5).

The process of the decomposition was also proved by the SEM images and UV spectra of the nanoparticle before and after heating. Figure 9 gave a set of SEM photographs of the same nanoparticles heated successively to 340 (a), 400 (b), and 600 °C (c). The particles heated to 340 °C were aggregated to form secondly sized particles 0.8 μm in diameter, exhibiting porosity. The particles heated to 400 °C further aggregated into a solid with a smooth surface. This aggregation occurred when the nanoparticles were heated for a long time at any temperature in the domain from 250 to 400 °C.

Figure 10 shows the UV spectra of the unheated nanoparticle and the nanoparticle heated to 340 and 400 °C. The band of the dried film at 457 nm in the aqueous solution (curve (b))

Thermal Metallization of Coated Nanoparticles

J. Phys. Chem. B, Vol. 108, No. 39, 2004 **15031**
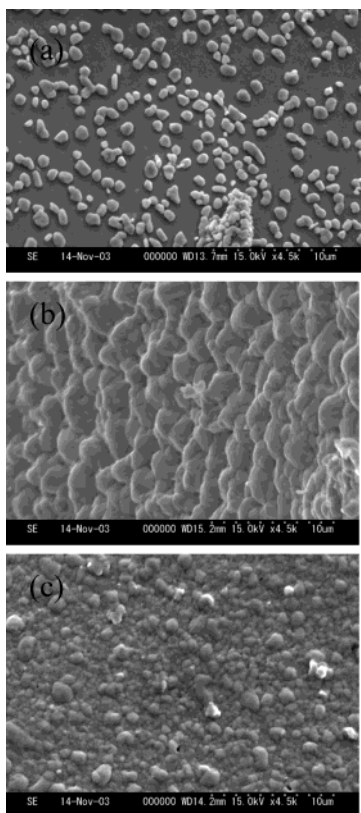
Figure 9. SEM images of the same nanoparticle heated succeedingly to (a) 340, (b) 400, and (c) 600 °C.

Figure 10. UV spectra of (a) the nanoparticle in the cyclohexane solution and (b) the unheated nanoparticle film on the ITO surface and the nanoparticle film heated to (c) 340 °C and (d) at 400 °C for 5 min in air.

was shifted from the band at 421 nm for nanoparticle-dissolved cyclohexane (curve (a)), which has been attributed[17] to Mie scattering. The band shift is due to a solvent effect. The nanoparticle heated to 250 °C shows almost the same spectrum (curve c)) as the film without heating. Therefore, the film ought to have the nanostructure for Mie scattering. It should necessarily be porous, as has been demonstrated not only with the lower density in Figure 8 ($250 < T < 340$ °C) but also with the SEM images in Figure 9. The nanoparticle heated to over 340 °C (curve (d)) shows no adsorption. The drastic variation in the disappearance of the absorption band may be due to changes in the porous silver by Mie scattering into silver bulk crystals.

Conclusions

The silver stearate-coated nanoparticle was metallized into bulk silver at 340 °C, which is much lower than the melting point of bulk silver (960 °C). The low-temperature metallization of the nanoparticle was due to the decomposition of silver stearate in the shell into silver metal and gas rather than the

actual melting of silver metal. The kinetics was first order with respect to silver stearate with an activation energy of 111 kJ mol^{-1}. This metallization can be discriminated against the low-temperature fusion of nanoparticles owing to large surface energy on the nanometer-scaled curvature.

The metallization of the nanoparticle occurred in two steps, one being the decomposition of silver stearate to porous silver retaining the nanostructure for $200 < T < 340$ °C and the second being the fused and sintered nanostructure to bulk silver crystal at temperatures greater than 340 °C. The first step was evidenced by FTIR, voltammetry, and the density measurement, and the second step was confirmed by UV spectroscopy, the density measurement, and the SEM images.

References and Notes

(1) (a) Dick, K.; Dhanasekaran, T.; Zhang, Z. Y.; Meisel, D. *J. Am. Chem. Soc.* **2002**, *124*, 2312. (b) Link, S.; Wang, Z. L.; El-Sayed, M. A. *J. Phys. Chem. B* **2000**, *104*, 7867. (c) Gao, S. M.; Xie, Y.; Zhu, L. Y.; Tian, X. B. *Inorg. Chem.* **2003**, *42*, 5442. (d) Martin, J. E.; Odinek, J.; Wilcoxon, J. P.; Anderson, R. A.; Provencio, P. *J. Phys. Chem. B* **2003**, *107*, 430. (e) Bachels, T.; Guntherodt, H. J.; Schafer, *Phys. Rev. Lett.* **2000**, *85*, 1250. (f) Wuelfing, W. P.; Zamborimi, F. P.; Templeton, A. C.; Wen, X. G.; Yoon, H.; Murray, R. W. *Chem. Mater.* **2001**, *13*, 87. (g) Luo, J.; Jones, V. W.; Maye, M. M.; Han, L.; Kariuki, N. N.; Zhong, C. J. *J. Am. Chem. Soc.* **2002**, *124*, 13988. (h) Luo, J.; Maye, M. M.; Han, L.; Kariuki, N. N.; Jones, V. W.; Lin, Y. H.; Engelhard, M. H.; Zhong, C. J. *Langmuir* **2004**, *20*, 4254.

(2) (a) Sun, S.; Murray, C. B.; Weller, D.; Folks, L.; Moser, A. *Science* **2000**, *287*, 1989. (b) Dai, Z.; Sun, S. Wang, Z. L. *Nano Lett.* **2001**, *1*, 443. (c) Humann, H.; Woods, S. I.; Sun, S. *Nano Lett.* **2003**, *3*, 1643. (d) Ashavani, K.; Chinmay, D.; Murali, S. *Appl. Phys. Lett.* **2001**, *79*, 3314. (e) Chinmay, D.; Anamika, G.; Murali, S. *Nano Lett.* **2002**, *2*, 365. (f) Harrell, J. W.; Wang, S.; Nikles, D. E.; Chen, M. *Appl. Phys. Lett.* **2001**, *79*, 4393. (g) Weller, D.; Moster, A.; Folkes, L.; Best, M. E.; Le, W.; Toney, M. F.; Shcweickert, M.; Thiele, J. L.; Doerner, M. F. *IEEE Trans. Magn.* **2000**, *36*, 10. (h) Kang, S. S.; Harrell, J. W.; Nikles, D. E. *Nano Lett.* **2002**, *2*, 1033.

(3) (a) Takami, A.; Kurita, H.; Koda, S. *J. Phys. Chem. B* **1999**, *103*, 1226. (b) Chang, S.; Shih, C.; Chen, C.; Lai, W.; Wang, C. R. C. *Langmuir* **1999**, *15*, 701. (c) Link, S.; Burda, C.; Nikoobakht, B.; El-Sayed, M. A. *J. Phys. Chem. B* **2000**, *104*, 6152. (d) Fujiwara, H.; Yanagida, S.; Kamat, P. V. *J. Phys. Chem. B* **1999**, *103*, 2589. (e) Link, S.; Wang, Z. L.; El-Sayed, M. A. *J. Phys. Chem. B* **1999**, *103*, 3529. (f) Shipwasy, A. N.; Katz, E.; Willner, I. *ChemPhysChem* **2000**, *1*, 18.

(4) Takagi, M. *J. Phys. Soc. Jpn.* **1954**, *9*, 359.

(5) Buffat, Ph.; Borel, J. P. *Phys Rev. A* **1976**, *130*, 2287.

(6) Castro, T.; Reifenberger, R.; Choi, E.; Andres, P. *Phys. Rev. B* **1990**, *42*, 8548.

(7) Schmidt, M.; Kusche, R.; Kromueller, W.; Von Issendorf, B.; Haberland, H. *Phys. Rev. Lett.* **1996**, *79*, 99.

(8) Lai, S.; Guo, J. Y.; Petrova, V.; Ramamath, G.; Allen, L. H. *Phys. Rev. Lett.* **1996**, *77*, 99.

(9) Shvartotsburg, A. A.; Jarrold, M. F. *Phys. Rev. Lett.* **2000**, *85*, 2530.

(10) Pawlow, P. Z. *Phys. Chem.* **1909**, *65*, 545.

(11) (a) Reiss, H.; Wilson, I. B. *J. Colloid. Sci.* **1948**, *3*, 551. (b) Borel, J.-P. *Surf. Sci.* **1981**, *106*, 1. (c) Ross, J.; Andress, R. P. *Surf. Sci.* **1981**, *106*, 11. (c) Shimizu, Y.; Sawada, S.; Ikeda, K. S. *Eur. Phys. J. D* **1998**, *4*, 365. (d) Peters, K. F.; Cohen, J. B.; Chung, Y.-W. *Phys. Rev. B* **1998**, *57*, 13430. (e) Sheng, H. W.; Lu, K; Ma, E. *Nanostruct. Mater.* **1998**, *10*, 865. (f) Cleveland, C. L.; Luedtke, W. D.; Landman, U. *Phys. Rev. B* **1999**, *60*, 5065. (g) Maye, M. M.; Zheng, W.; Leibowitz, F. L.; Ly, N. K.; Zhong, C. J. *Langmuir* **2000**, *16*, 490. (h) Mayer, M. M.; Zhong, C. J. *Mater. Chem.* **2000**, *10*, 1895. (i) Zhao, S. J.; Wang, D. Y.; Cheng, D. Y.; Ye, H. Q. *J. Phys. Chem. B* **2001**, *105*, 12857.

(12) Kofman, R.; Cheyssac, P.; Aouaj, A.; Lereah, Y.; Deutscher, G.; B.-David, T.; Penisson, J. M.; Bourret, A. *Surf. Sci.* **1994**, *303*, 231.

(13) (a) Sakai, H. *Surf. Sci.* **1996**, *348*, 387. (b) Sakai, H. *Surf. Sci.* **1996**, *351*, 285.

(14) Beck, T. L.; Jellinek, J.; Berry, R. S. *J. Chem. Phys.* **1987**, *87*, 545.

(15) Honeycutt, J. D.; Andreson, H. C. *J. Phys. Chem.* **1987**, *91*, 4950.

(16) (a) Berry, R. S.; Iellinek, J.; Natanson, G. *Phys. Rev. A* **1987**, *91*, 4950. (b) Resis, H.; Mirabel, P.; Whetten, R. L. *J. Phys. Chem.* **1988**, *92*,

7241. (c) Wales, D. J.; Berry, R. S. *J. Chem. Phys*. **1990**, *92*, 4473. (d) Wales, D. J.; Berry, R. S. *J. Chem. Phys*. **1990**, *92*, 4283. (e) Mirabel, P.; Reiss, H,; Bowles. R. K. *Chem. Phys*. **2000**, *113*, 8200.

(17) Aoki, K.; Chen, J.; Yang, N. J.; Nagasawa, H. *Langmuir* **2003**, *19*, 9904.

(18) (a) Nagasawa, H.; Maruyama, M.; Komatsu, T.; Isoda, S.; Kobayashi, T. *Phys. Status Solidi A* **2002**, *191,* 67. (b) Kuwajima, S.; Okada, Y.; Yoshida, Y.; Abe, K.; Tanigaki, N.; Yamaguchi, T.; Nagasawa, H.; Sakurai, K.; Yase, K. *Colloids Surf., A* **2002**, *197,* 1. (c) Abe, K.; Hanada,

T.; Yamaguchi, T.; Takiguchi, H.; Nagasawa, H.; Nakamoto, M.; Yase, K. *Mol. Cryst. Liq. Cryst*. **1998**, *322,* 173. (d) Abe, K.; Hanada, T.; Yoshida, Y.; Tanigaki, N.; Takiguchi, H.; Nagasawa, H.; Nakamoto, M.; Yamaguchi, T.; Yase, K. *Thin Solid Films* **1998**, *327,* 524.

(19) Atkins, P. W. *Physical Chemistry*, 6th ed.; Oxford University Press, Oxford, England, 1998; pp 9−229.

(20) (a) Chrissafis, K. *Thermochim. Acta* **2004**, *411*, 7. (b) Srikanth, S.; Chakravortty, M. **2001**, *370*, 141. (c) Sonibare, O. O.; Egashira, R.; Adeosu, T. A. *Thermochim. Acta* **2003**, *405*, 195.